ACCOUNTS
of chemical research

Anion−π Interactions in Supramolecular Architectures

HELEN T. CHIFOTIDES* AND KIM R. DUNBAR*

Department of Chemistry, Texas A&M University, PO Box 30012, College Station, Texas 77842, United States

RECEIVED ON AUGUST 25, 2012

CONSPECTUS

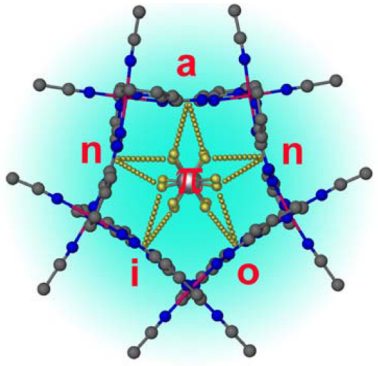

The study of the noncovalent force between π-acidic aromatic systems and anions, referred to as the anion−π interaction, has recently emerged as a new branch of supramolecular chemistry. The anion−π contact is complementary to the cation−π interaction, a prominent noncovalent force involved in protein structure and enzyme function. Until recently, the scientific community had overlooked the anion−π interaction due to its ostensibly counterintuitive nature. Pioneering theoretical studies in 2002, however, established that anion−π interactions are energetically favorable (∼20−70 kJ/mol) and prompted a flurry of reports in support of their existence. The interest in anion−π contacts was further fueled by the importance of anions in key chemical and biological processes and the involvement of π-rings in anion recognition and transport. Anion−π interactions hold great promise for the design of selective anion receptors, hosts or scaffolds, colorimetric sensors, and catalysts and may also affect biological functions. Currently, the area of anion−π research is highly topical in the scientific community and on a meteoric rise in the chemical literature. This Account highlights our leading findings in this burgeoning area.

Our work has focused on comprehensive investigations of several unprecedented supramolecular systems, in which the anions and their close anion−π contacts are the driving elements of the final architectures. We surveyed several heterocyclic π-acidic aromatic systems amenable to anion−π contacts and explored the subtle interplay between ligand π-acidity, anion identity, and metal ions in mediating the ensuing self-assembled architectures.

The reactions we performed between solvated first-row transition metal ions and the π-acidic ligands bptz (3,6-bis(2-pyridyl)-1,2,4,5-tetrazine) or bmtz (3,6-bis(2-pyrimidyl)-1,2,4,5-tetrazine) resulted in unprecedented metallacycles. Our investigations revealed that the identity of the encapsulated ion dictates the metallacycle nuclearity and close anion−π contacts are critical for the metallacycle stability. Our X-ray crystallographic, NMR spectroscopic, and mass spectrometric (MS) studies demonstrated that the tetrahedral ($[BF_4]^-$, $[ClO_4]^-$) and octahedral ($[SbF_6]^-$, $[AsF_6]^-$, $[PF_6]^-$) anions template discrete molecular squares and pentagons, respectively. The metal ions occupy the vertices, and bptz or bmtz moieties span the edges of the metallacycles. The encapsulated anions occupy the π-acidic cavities of the metallacycles and establish multiple close directional F/O$\cdots C_{tetrazine}$ contacts with the edges. The observation of notable ^{19}F solid-state NMR chemical shifts reflects the short contacts of the encapsulated anions, findings that we corroborated by DFT calculations. The solution NMR data support the conclusion that *bona fide* metallacycle templation and interconversion between the metallacycles in solution occurs *only* in the presence of the appropriate anions. The NMR, MS, and CV data underscore the remarkable metallapentacycle stability despite the angle strain inherent in pentagons formed by octahedral metal ions. The low anion activation energies of encapsulation ($\Delta G^{\ddagger} \sim 50$ kJ/mol) suggest that anion−π contacts assist the anion templation.

We also studied reactions of Ag(I)X (X^- = $[PF_6]^-$, $[AsF_6]^-$, $[SbF_6]^-$, $[BF_4]^-$) with bptz or bppn (3,6-bis(2-pyridyl)-1,2-pyridazine) to assess the effect of the ligand π-acidity on the preferred structures. The X-ray data revealed that the higher π-acidity of the tetrazine ring in bptz leads to propeller-type products $[Ag_2(bptz)_3]^{2+}$ exhibiting prominent short anion−π contacts. By contrast, the less π-acidic bppn preferentially favors grids $[Ag_4(bppn)_4]^{4+}$ which exhibit maximized π−π interactions.

Finally, we explored the reactions of the extended π-acidic heterocycle HAT(CN)$_6$ (1,4,5,8,9,12-hexaazatriphenylene-hexacarbonitrile) with the Cl^-, Br^-, I^- ions which lead to highly colored solutions/crystals. X-ray crystallographic studies of the HAT(CN)$_6$/halide complexes revealed unprecedented multisite short peripheral charge-transfer and centroid anion−π contacts. In solution, the charge-transfer contacts were evidenced by electronic absorption, ^{13}C and halogen NMR, as well as MS data. The distinctly colored complex entities exhibit extraordinarily high association constants, which render them promising for anion-sensing receptor applications.

Published on the Web 03/11/2013 www.pubs.acs.org/accounts
10.1021/ar300251k

1. Introduction

The ubiquitous presence of noncovalent interactions involving aromatic moieties in chemical and biological processes grants them a prominent role in the fascinating field of supramolecular chemistry. In fact, the topic of weak interactions involving π-systems is at the forefront of research in major interdisciplinary thrust areas spanning materials science, catalysis, crystal engineering, biology and medicine.[1] In the realm of biological sciences, a plethora of cases reveal that noncovalent aromatic interactions, (for example, π−π, CH−π, cation−π, and lone pair−π) orchestrate the structures of biomolecules and play a pivotal role in many vital functions such as DNA/RNA stacking, protein folding, protein−ligand recognition, and drug−receptor interactions. A perusal of the literature reveals numerous pertinent examples, for example, π−π stacking, cation-π and O−H···π interactions stabilize the complex of the enzyme acetylcholinesterase with the Alzheimer's disease drug E2020,[1] and cation−π interactions play a critical role in the molecular recognition process at the binding sites of a diverse array of proteins.[2]

The aforementioned arsenal of noncovalent contacts associated with aromatic rings was recently augmented by a newly recognized noncovalent force between π-acidic charge-neutral aromatic rings and anions, namely, the anion−π interaction (Figure 1). The term anion−π was coined by Deyà et al. in 2002,[3] but the origins of attractive interactions between anions and π-acidic aromatic rings are found in earlier reports.[4,5] Thereafter, three almost simultaneous pioneering theoretical studies by Deyà et al.,[3] Mascal et al.,[6] and Alkorta et al.,[7] reported in 2002, established that anion−π interactions are energetically favorable (∼20−70 kJ/mol,[8,9] i.e., comparable in energy to cation−π interactions and moderate-strong hydrogen bonds) and heralded the nascence of this field. Since these reports, a surge of theoretical and experimental investigations in support of anion−π contacts ensued and are detailed in several state-of-the-art Review articles on the topic, which collectively demonstrate the trends in the field.[8−12]

In light of the omnipresence of anions in many key chemical and biochemical systems and the involvement of π-rings in molecular anion recognition and transport,[13] anion−π contacts are expected to be prominent players in a wide range of pivotal processes. The widespread importance of cation−π interactions in proteins notwithstanding,[2] anion−π interactions recently came to light in several enzymes and other proteins.[14−17] Furthermore, the closely related C−Cl/C-Br···π interactions were recently found to enhance

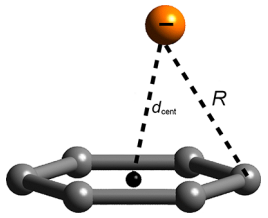

FIGURE 1. Schematic representation of π-system in close contact with anion.

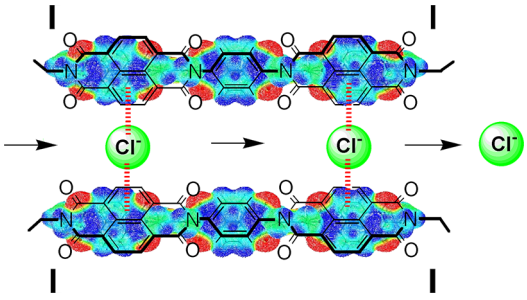

FIGURE 2. Transmembrane anion−π slide for chloride transport. Adapted with permission from ref 32 (c). Copyright 2006 American Chemical Society.

protein−ligand binding affinity[18] and lone pair···π interactions to stabilize Z-DNA.[19] Currently, the scientific community is focusing increasing attention on the great potential *vis-à-vis* anion−π interactions and the exciting opportunities they present for the design of highly selective anion receptors,[12,13,20−22] novel colorimetric sensors,[12,23−26] selective hosts[27] or scaffolds[20,23] for anion recognition,[13,28−30] catalysts and other materials.[31] A few groups have made impressive strides toward key applications; for example, Matile et al. recently reported pioneering studies which unveiled π-acidic naphthanediimide (NDI) lipid bilayer rods (synthetic transmembrane anion−π slides) enabling anion transport via anion−π interactions (Figure 2);[32] in light of the physiological relevance of biological chloride channels, these developments pave the way for the treatment of channelopathies such as cystic fibrosis.[13]

As part of our broad interest in supramolecular chemistry, we have been exploring several π-acidic aromatic systems such as bptz:3,6-bis(2-pyridyl)-1,2,4,5-tetrazine, bmtz: 3,6-bis(2-pyrimidyl)-1,2,4,5-tetrazine, and bppn:3,6-bis-(2-pyridyl)-1,2-pyridazine, which are amenable to short contacts with anions. Comprehensive studies undertaken by our group resulted in the isolation of unprecedented metallacycles,[33−35] grids, and propeller-type[36,37] frameworks in which the anions and their close contacts with the N-heterocyclic ligands facilitate the self assembly process and control the structures of the final supramolecular entities. We embarked on a quest to gain insight into the subtle

interplay between anion identity, ligand π-acidity, and metal ion in mediating the structures and properties of the ensuing metallasupramolecular architectures. Our data provide compelling evidence, unique to the area of anion-assisted chemistry, that the metallacycles *only* form in the presence of suitable anions. Formation of these polygons occurs via synergistic anion−π interactions, which are an integral part of metallacycle templation, with low activation energies of anion encapsulation (∼50 kJ/mol). In another recent study, we targeted an extended π-acidic molecule, namely, HAT(CN)$_6$ (1,4,5,8,9,12-hexaazatriphenylene-hexacarbonitrile), an excellent platform for effective halide recognition and a promising colorimetric anion sensor, with the halide ions driving the spontaneous self-assembly of the sandwich-like complexes.[23] This Account highlights our most significant advances in the aforementioned areas. To enhance understanding of the topic by nonspecialist readers, we first describe the basic characteristics of anion−π interactions.

2. Physical Nature of Anion−π Interactions

In contrast to cation binding to aromatic systems, the anion−π interaction was previously overlooked, presumably due to its counterintuitive nature. This ostensibly unfavorable interaction with a negative π-surface can become attractive, however, for aromatics with electron-withdrawing substituents or N-heterocyclic rings. Extensive studies have shown that in general electrostatic and anion-induced polarization contributions dominate anion−π interactions,[9] but recently an alternate driving force was proposed for substituted benzene rings.[38] The electrostatic component correlates strongly with the magnitude of the ring permanent quadrupole moment Q_{zz}, which describes the charge distribution on both sides of the aromatic plane, for example, $Q_{zz} = -8.48$ and $+9.50$ B for benzene and hexafluorobenzene, respectively (1 B = 3.336×10^{-40} C m^2; Figure 3, upper panel). Aromatic rings with large positive quadrupole moments establish strong anion−π interactions, for example, Q_{zz}(dicyano NDI) = +39.2 B.[32b] Anion-induced polarization arises from the interaction of the anion with the π-system induced dipole and has significant contributions for molecules with high polarizability or extended π-systems, for example, $\alpha_{\parallel}$(*s*-tetrazine) = 58.7 or $\alpha_{\parallel}$(HAT) = 54.03 au, respectively.[8,9]

Electrostatic potential (ESP) maps have been widely used in the analyses of noncovalent interactions.[38] The ESP at a selected location near a molecule is a measure of the electrostatic energy that a positive unit point charge would experience at that location. The point charge is attracted to negative and repelled by positive potentials, depicted typically as red and blue on color plots; these ESPs usually correspond to electron-rich and electron-poor regions, respectively, for example, benzene and hexafluorobenzene have reversed electrostatic potentials (Figure 3, lower panel).

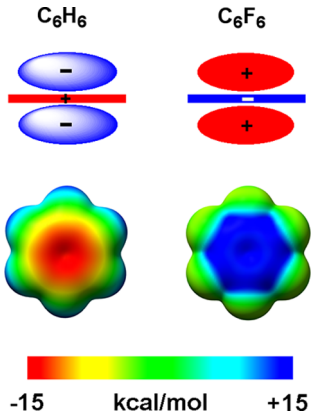

FIGURE 3. Schematic representations of quadrupole moments (upper) and ESP maps[38] (lower): (left) benzene and (right) hexafluorobenzene.

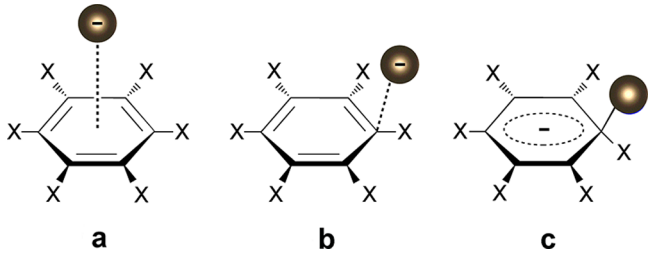

FIGURE 4. Anion interaction types with π-systems (a) anion−π, (b) anion-donor−π-acceptor, and (c) strongly covalent σ interaction.

3. Interaction Motifs of Anions with π-Systems

Depending on the anion and π-system types, three interaction modes are possible between a π-acidic aromatic ring and an anion located above it (Figure 4): (a) noncovalent anion−π contact with the anion centered or displaced from the ring centroid,[9] (b) anion-donor−π-acceptor interaction with positioning of the anion over the π-system periphery,[39,40] and (c) strongly covalent σ interaction or Meisenheimer intermediate.[9,39,40]

An empirical indication of the anion−π interaction strength is the distance d_{cent} or R (Figure 1); increasing the anion/aromatic plane distance by moving the anion in a direction vertical to the plane results in weaker interactions.[9] The latest proposed broader criterion to invoke an anion−π interaction is for the anion to be located above the aromatic ring region at anion to carbon atom distances ≤ sum of van der Waals radii (ΣR_{vdW}) + 0.8 Å.[9,11]

Theoretical studies have aimed at probing the detailed characteristics and preferred geometries for various aromatic ligands with different anions.[3,6,7,9,39,40] Strong σ-complexes

are usually formed with nucleophilic anions, for example, $[RO]^-$, $[CN]^-$, F^-, and π-acidic arenes.[6,39,40] Anion−π complexes are most likely to occur with large, charge-diffuse anions, for example, $[ClO_4]^-$, $[BF_4]^-$, $[PF_6]^-$, and arenes of moderate electron affinity.[11] Mononuclear anions such as Cl^- and Br^- establish both anion-donor−π-acceptor and anion−π contacts with arenes of moderate electron affinity, for example, triazine.[39,40] As the electron affinity of the arene increases, however, anion-donor−π-acceptor complexes are preferred, for example, halide complexes of tetracyanobenzene, tetracyanopyrazine, *o*-chloranil,[39−41] which exhibit η^1 or η^2 hapticities and several close anion-ring contacts (Figure 5). Moreover, the positioning of polyatomic anions, for example, $[BF_4]^-$, $[PF_6]^-$, $[SbF_6]^-$, $[ClO_4]^-$, varies with ring symmetry and anion geometry; several short F/O contacts are typically established with the π-acidic aromatic rings,[11,16] as a search of the CSD indicates and also is the case for our assemblies.

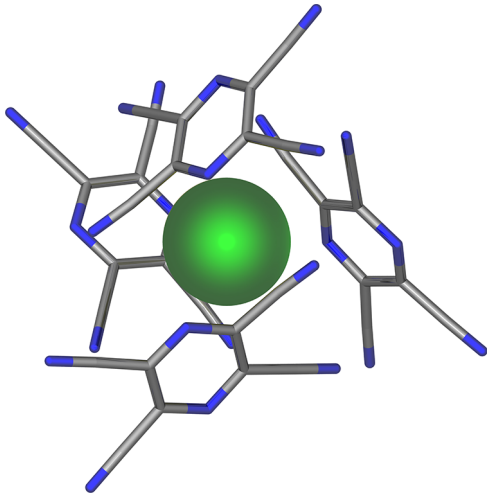

FIGURE 5. Tetracyanopyrazine crystallized with Cl^-.[41]

4. Anion−π Interactions in Templated Metallacycles with π-Acidic Cavities

Noncovalent interactions are powerful tools for the design and control of supramolecular entities.[42,43] In this realm, a useful approach entails combining the assets of coordination bonds[43] and the convenience of a template to organize the molecular building blocks to favor a desired supramolecular architecture. Of particular relevance to our work is the templating ability of anions[44] in the self-assembly of metallasupramolecular systems, which has only recently been appreciated. Armed with this approach, we launched a comprehensive investigation of the anion-templated discrete molecular squares $[\{M_4(bptz)_4(CH_3CN)_8\}\subset X][X]_7$, (M = Ni, Fe, Zn; $[X]^- = [BF_4]^-, [ClO_4]^-$) and pentagons $[\{Ni_5(bptz)_5(CH_3CN)_{10}\}\subset SbF_6][SbF_6]_9$, $[Fe_5(bptz)_5(CH_3CN)_{10}][Y]_{10}$ ($[Y]^- = [SbF_6]^-, [AsF_6]^-, [PF_6]^-$), and $[\{Fe_5(bmtz)_5(CH_3CN)_{10}\}\subset SbF_6][SbF_6]_9$, which were isolated in high yields. The central tetrazine rings of the ligands are highly π-acidic (Figure 6) and thus amenable to anion−π interactions with the encapsulated anions which, as evidenced by our studies, act as templating elements and are critical for the formation of one metallacycle over another. The anion resides in the metallacycle cavity, and the nuclearity is dictated by the specific anion present during the self-assembly process. In Table 1, a compendium of the metallacycles characterized by X-ray crystallography to date is provided;[33−35,45,46] the relatively small tetrahedral $[BF_4]^-$ and $[ClO_4]^-$ anions template molecular squares (Scheme 1, Figure 7), whereas the larger octahedral $[SbF_6]^-$ anion exclusively favors unprecedented metallapentacycles (Scheme 1, Figure 8). Combined data from X-ray crystallography, ^1H and ^{19}F NMR spectroscopies, cyclic voltammetry (CV), and mass spectrometry (MS) reveal that the templating anions play a decisive role in this

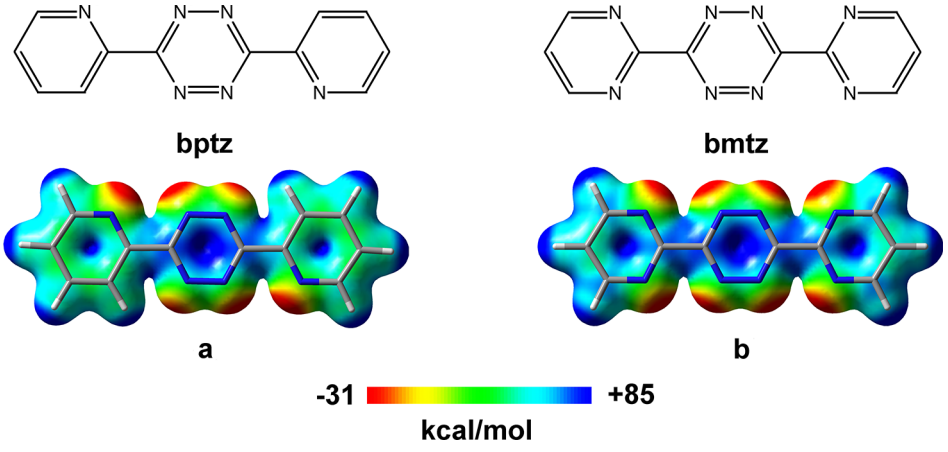

FIGURE 6. Schematic representations and ESP maps of (a) bptz and (b) bmtz calculated with B3LYP/6-31+G(d,p).[48]

TABLE 1. Crystallographically Determined Metallacycles and Their Anion−π Contacts

metallacycle	templating anion(s)	F/O···C anion−π contacts with tetrazine rings (Å)	average anion−π contact (Å)	ref
$[\{Ni_4(bptz)_4(CH_3CN)_8\}\subset BF_4][BF_4]_7$	$[BF_4]^-$ [a]	2.69, 2.82, 2.87, 2.98, 2.99, 3.05	2.90[b]	33, 46
$[\{Ni_4(bptz)_4(CH_3CN)_8\}\subset ClO_4][ClO_4]_7$	$[ClO_4]^-$ [a]	2.83, 2.90, 2.99, 3.01, 3.18, 3.20	3.02[c]	33
$[\{Ni_5(bptz)_5(CH_3CN)_{10}\}\subset SbF_6][SbF_6]_9$	$[SbF_6]^-$ [a]	2.73, 3.02, 3.03, 3.04, 3.10, 3.16	3.01[b]	33, 45
$[\{Ni_4(bptz)_4(CH_3CN)_8\}\subset I][SbF_6]_7$	I^-	3.275, 3.517	3.39[d]	33
$[\{Ni_4(bptz)_4Br_7(CH_3CN)\}\subset Br_3]$	$[Br_3]^-$	3.297, 3.337, 3.499, 3.521	3.41[d]	33
$[\{Ni_4(bptz)_4(CH_3CN)_8\}\subset BF_4][PF_6][SbF_6]_6$	$[BF_4]^-$ [a]	2.75, 2.83, 2.88, 2.93, 3.07	2.90[b]	33
$[\{Zn_4(bptz)_4(CH_3CN)_8\}\subset BF_4][BF_4]_7$	$[BF_4]^-$	2.73, 2.79, 2.89, 3.08, 3.18	2.93[b]	33
$[\{Zn_4(bptz)_4(CH_3CN)_4(H_2O)_4\}\subset ClO_4][ClO_4]_7$	$[ClO_4]^-$	2.89, 3.03, 3.05, 3.07	3.00[c]	47
$[\{Co_4(bptz)_4(CH_3CN)_8\}\subset BF_4][BF_4]_7$	$[BF_4]^-$	2.73, 2.79, 2.88, 2.89	2.82[b]	48
$[\{Fe_4(bptz)_4(CH_3CN)_8\}\subset BF_4][BF_4]_7$	$[BF_4]^-$ [a]	2.74, 2.78, 2.80, 2.83, 2.86, 2.88, 2.93, 2.95	2.84[b]	35
$[\{Fe_5(bptz)_5(CH_3CN)_{10}\}\subset 2SbF_6][SbF_6]_8$	$[SbF_6]^-$ [a,e]	2.81, 2.83, 2.89, 2.93, 2.96, 3.03	2.91[b]	34, 35
$[\{Fe_5(bmtz)_5(CH_3CN)_{10}\}\subset SbF_6][SbF_6]_9$	$[SbF_6]^-$	2.79, 2.81, 2.93, 2.94, 3.00, 3.09	2.93[b]	34

[a] Anion(s) disordered between two positions. [b] ΣR_{vdW} F···C: 3.17 Å. [c] ΣR_{vdW} O···C: 3.22 Å. [d] Halide···tetrazine ring centroid distances; ΣR_{vdW} I···C: 3.68 Å; ΣR_{vdW} Br···C: 3.55 Å. [e] Two encapsulated $[SbF_6]^-$ anions.

SCHEME 1

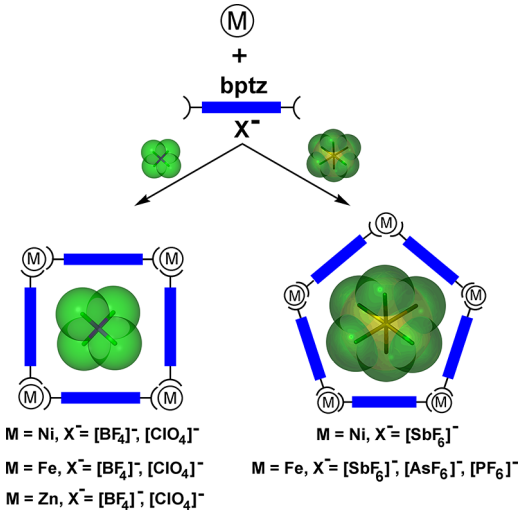

chemistry by stabilizing one particular cyclic structure over another due to favorable additive anion−π interactions with the π-acidic cavities spanned by bptz or bmtz; to our knowledge, metallacycle templation mediated by anion−π contacts has not been previously documented in the literature.

The influence of the size, shape and geometry of the anions notwithstanding, there also is a subtle interplay between these factors and the potential of the anion to establish strong anion−π contacts with the π-acidic moieties in the metallacycle cavities. Indeed, careful examination of the metallacycle X-ray structural parameters reveals that the encapsulated anions establish multiple close contacts with the tetrazine rings. For example, in the molecular squares $[\{Ni_4(bptz)_4(CH_3CN)_8\}\subset I]^{7+}$ or $[\{Ni_4(bptz)_4Br_7(CH_3CN)\}\subset Br_3]$, the encapsulated spherical I^- or linear $[Br_3]^-$ ions establish several d_{cent} halide···tetrazine centroid contacts shorter by

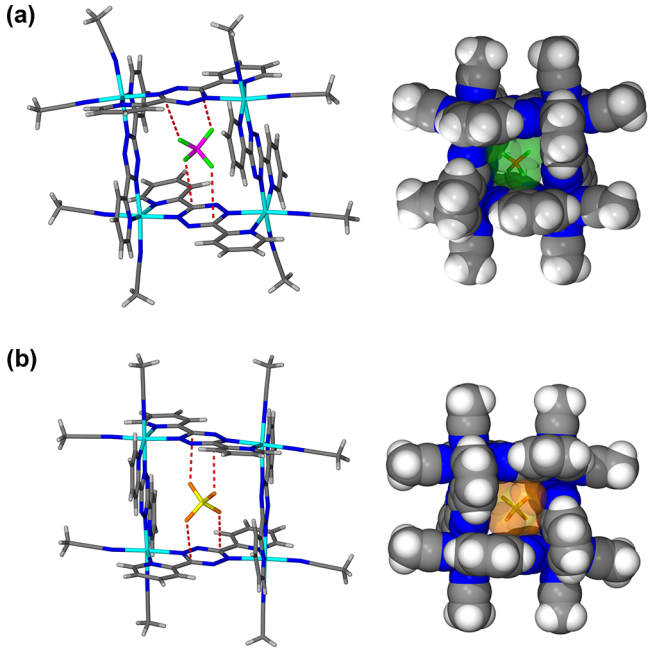

FIGURE 7. Short anion−π contacts in X-ray structures of squares: (a) $[\{Ni_4(bptz)_4(CH_3CN)_8\}\subset BF_4]^{7+}$ and (b) $[\{Ni_4(bptz)_4(CH_3CN)_8\}\subset ClO_4]^{7+}$. Adapted with permission from ref 33. Copyright 2005 American Chemical Society.

0.30 or 0.15 Å than ΣR_{vdW} I···C (3.68 Å) or ΣR_{vdW} Br···C (3.55 Å), respectively (Figure 9, Table 1).[33]

It is noteworthy that, for the metallacycles templated by $[BF_4]^-$, $[ClO_4]^-$ (Figures 7 and 10A), or $[SbF_6]^-$ (Figure 8), for example, the encapsulated polyatomic anions are embraced by the π-acidic cavities and optimally positioned in a fashion allowing for the maximum number and strength of short directional F/O···$C_{tetrazine}$ additive anion−π contacts with the π-acidic tetrazine C atoms of the cavities at distances 2.8−3.0 Å, that is, up to 0.4 Å shorter than ΣR_{vdW}F/O···C (Table 1).[33−35,45,46] Additionally, for several

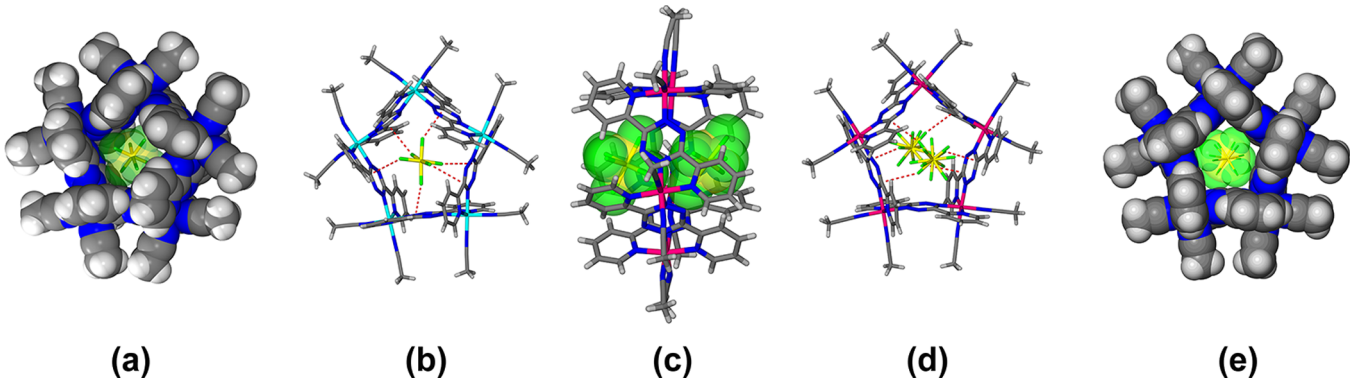

FIGURE 8. Short anion−π contacts in pentagonal X-ray structures: (a,b) $[\{Ni_5(bptz)_5(CH_3CN)_{10}\}\subset SbF_6]^{9+}$,[33] (c−e) $[\{Fe_5(bptz)_5(CH_3CN)_{10}\}\subset 2SbF_6]^{8+}$.[34,35]

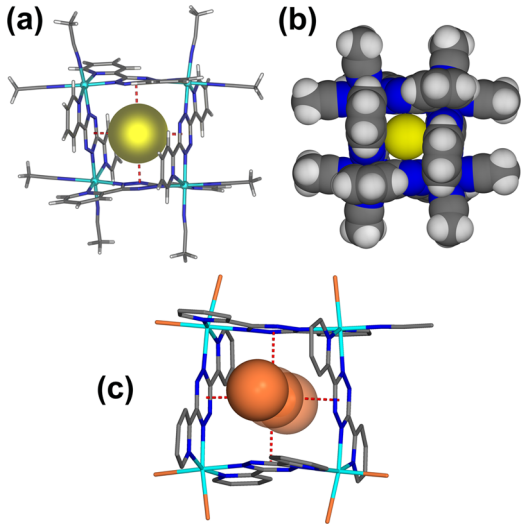

FIGURE 9. Short anion−π contacts in square X-ray structures: (a, b) $[\{Ni_4(bptz)_4(CH_3CN)_8\}\subset I]^{7+}$; (c) $[\{Ni_4(bptz)_4Br_7(CH_3CN)\}\subset Br_3]$.[33]

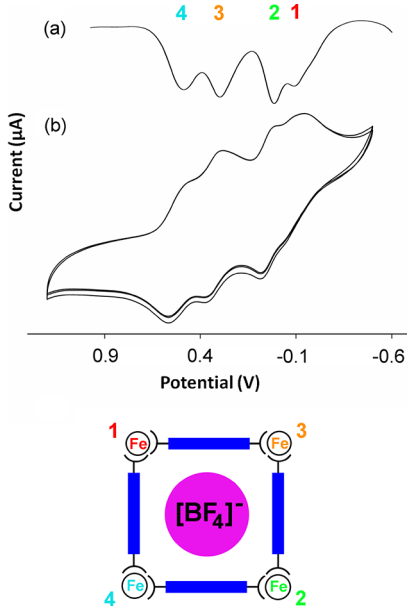

FIGURE 11. (a) Differential pulse and (b) cyclic voltammograms for $[Fe_4(bptz)_4(CH_3CN)_8][BF_4]_8$. Adapted with permission from ref 35. Copyright 2013 American Chemical Society.

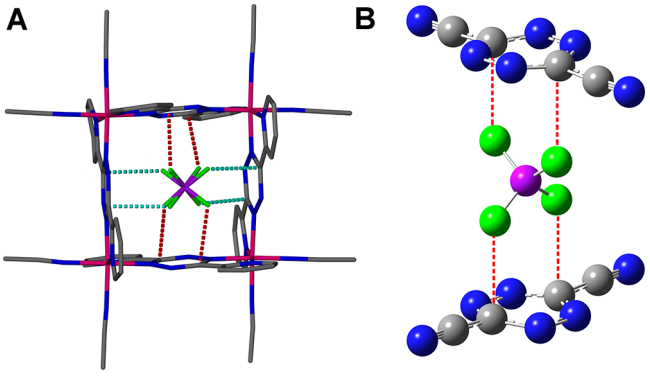

FIGURE 10. (A) X-ray structure of $[\{Fe_4(bptz)_4(CH_3CN)_8\}\subset BF_4]^{7+}$, (B) $C_2N_4(CN)_2\cdots[BF_4]^-\cdots C_2N_4(CN)_2$ adduct optimized with B3LYP/6-31+G(d); directional anion−π contacts depicted with dashed lines. Adapted with permission from ref 35. Copyright 2013 American Chemical Society.

of the aforementioned metallacycle structures, the optimal anion positioning in the cavity *vis-à-vis* the opposing tetrazine ring carbon atoms and the $F\cdots C_{tetrazine}$ distances were corroborated by DFT calculations performed for the binary adducts $C_2N_4R_2\cdots[X]^-\cdots C_2N_4R_2$ (R = F, CN; $[X]^- = [BF_4]^-$, $[PF_6]^-$), for example, Figure 10B.[35] Additionally, the short $F\cdots C_{tetrazine}$ anion−π interactions with the π-acidic cavities in $[Fe_4(bptz)_4(CH_3CN)_8][BF_4]_8$, $[Zn_4(bptz)_4(CH_3CN)_8][BF_4]_8$, and $[Fe_5(bptz)_5(CH_3CN)_{10}][SbF_6]_{10}$ were detected by unprecedented solid-state ^{19}F MAS NMR studies, which revealed downfield-shifted resonances $\Delta\delta(^{19}F) \sim 4$ ppm for the encapsulated versus the peripheral anions, in accord with their involvement in noncovalent contacts in the solid state.[35]

The stability of the aforementioned discrete, intact metallacycles in solution was established by mass spectrometry and, for the Fe(II) square/pentagons, by electrochemistry as

SCHEME 2

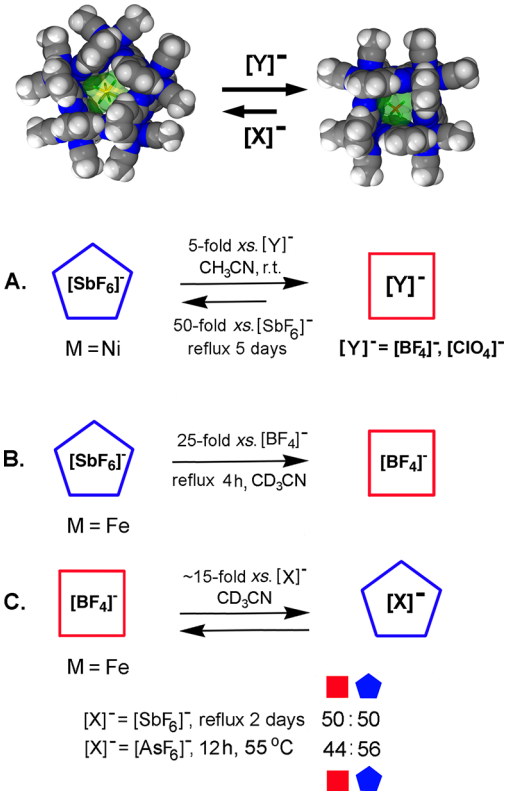

well; the cyclic voltammograms of the Fe(II) metallacycles exhibit several sequential reversible metal-centered oxidation processes (for example, Figure 11) and, interestingly, a shift of the bptz reduction features to more negative potentials versus free bptz. The latter is counterintuitive unless one considers that the ligand π-acidity has decreased due to anion−π contacts.[33−35] The polygon stability, especially of the pentagons, is remarkable given the inherent strain due to the incongruity between octahedral metal ion and internal pentagon angles (90° vs 108°). The intrinsic instability of the pentagons[43] is apparently overcome by the *inward bowing* of the central tetrazine moieties, to alleviate angle strain as well as to establish multiple short anion−π contacts with the encapsulated $[SbF_6]^-$ anions (evidenced in $[\{Ni_5(bptz)_5(CH_3CN)_{10}\}\subset SbF_6][SbF_6]_9$,[33,45] $[\{Fe_5(bptz)_5(CH_3CN)_{10}\}\subset 2SbF_6][SbF_6]_8$, and $[\{Fe_5(bmtz)_5(CH_3CN)_{10}\}\subset SbF_6][SbF_6]_9$; Figure 8).[33−35]

The decisive role of the anions in stabilizing specific Ni(II) polygons was further probed by interconversion studies performed by mass spectrometry and X-ray crystallography: $[\{Ni_5(bptz)_5(CH_3CN)_{10}\}\subset SbF_6][SbF_6]_9$ is readily converted to $[\{Ni_4(bptz)_4(CH_3CN)_8\}\subset BF_4][BF_4]_7$ or $[\{Ni_4(bptz)_4(CH_3CN)_8\}\subset ClO_4][ClO_4]_7$ with an excess of the corresponding tetrahedral anion, whereas the reverse transformation of the intrinsically more stable molecular squares to the less stable pentagon

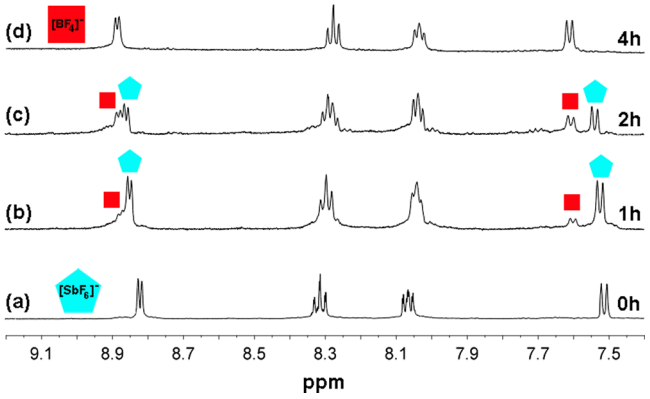

FIGURE 12. ^{1}H NMR spectra in CD_3CN for conversion of $[Fe_5(bptz)_5(CH_3CN)_{10}][SbF_6]_{10}$ to $[Fe_4(bptz)_4(CH_3CN)_8][BF_4]_8$: (a) $[Fe_5(bptz)_5(CH_3CN)_{10}][SbF_6]_{10}$ (b-d) refluxed with a 25-fold excess of $[n\text{-}Bu_4N][BF_4]$ for specified time. Adapted with permission from ref 35. Copyright 2013 American Chemical Society.

requires refluxing for 5 days, with a 50-fold excess of $[SbF_6]^-$ ions in CH_3CN, and is only partial (Scheme 2A).[33] Conversely, abstraction of the iodide from $[\{Ni_4(bptz)_4(CH_3CN)_8\}\subset I][SbF_6]_7$ with $TlPF_6$, leads to transformation of the square to the less stable pentagon $[\{Ni_5(bptz)_5(CH_3CN)_{10}\}\subset SbF_6][SbF_6]_4[PF_6]_5$,[33] a finding which suggests that a square without the appropriate encapsulated ion is unstable.

The higher stability of the Ni(II) squares versus the pentagon notwithstanding, it is notable that the relative polygon stability for the Fe(II) congeners favors the pentagons. Solution interconversion studies between the low-spin Fe(II) metallacycles under the competing influence of the anions, conducted by ^{1}H NMR spectroscopy, underscore the remarkable stability of the metallapentacycles and the critical role of the anion in their templation.[35] Surprisingly, $[\{Fe_5(bptz)_5(CH_3CN)_{10}\}\subset 2SbF_6][SbF_6]_8$ is *not* converted to $[\{Fe_4(bptz)_4(CH_3CN)_8\}\subset BF_4][BF_4]_7$ by mere overnight stirring with 15-fold excess of $[n\text{-}Bu_4N][BF_4]$ in CD_3CN; rather refluxing for 4 h with a 25-fold excess of $[n\text{-}Bu_4N][BF_4]$ is required (Scheme 2B, Figure 12).[35] The high stability of $[\{Fe_5(bptz)_5(CH_3CN)_{10}\}\subset 2SbF_6][SbF_6]_8$ is further supported by the fact that an ~50:50 $[Fe_4(bptz)_4(CH_3CN)_8][BF_4]_8$:$[Fe_5(bptz)_5(CH_3CN)_{10}][SbF_6]_{10}$ mixture is formed upon refluxing $[\{Fe_4(bptz)_4(CH_3CN)_8\}\subset BF_4][BF_4]_7$ with an excess of $[n\text{-}Bu_4N][SbF_6]$ for 2 days (Scheme 2C, Figure 13).[35]

The higher stability of $[\{Fe_5(bptz)_5(CH_3CN)_{10}\}\subset 2SbF_6][SbF_6]_8$ as compared to the Ni(II) congener, with respect to their corresponding conversions to squares with encapsulated $[BF_4]^-$ ions (Scheme 2, A and B), is attributed to the considerably smaller cavity size of the former (Table 2), which results in shorter by 0.1 Å and thus stronger anion−π interactions (Table 1). The subtle, yet decisive role of the

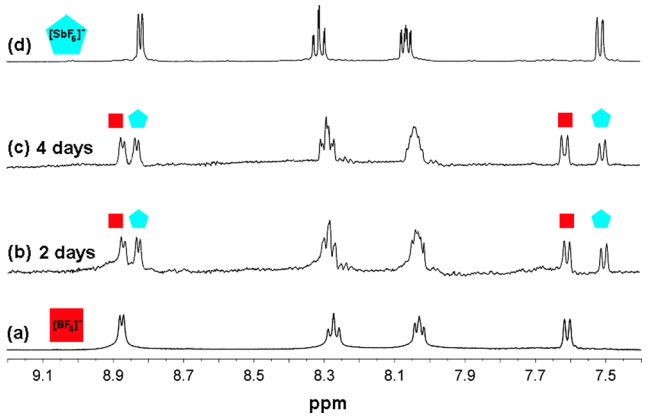

FIGURE 13. ^{1}H NMR spectra in CD_3CN for conversion of $[Fe_4(bptz)_4(CH_3CN)_8][BF_4]_8$ to $[Fe_5(bptz)_5(CH_3CN)_{10}][SbF_6]_{10}$ (a) $[Fe_4(bptz)_4(CH_3CN)_8][BF_4]_8$ (b-c) refluxed with a 16-fold excess of $[n\text{-}Bu_4N][SbF_6]$ for specified time (d) $[Fe_5(bptz)_5(CH_3CN)_{10}][SbF_6]_{10}$. Adapted with permission from ref 35. Copyright 2013 American Chemical Society.

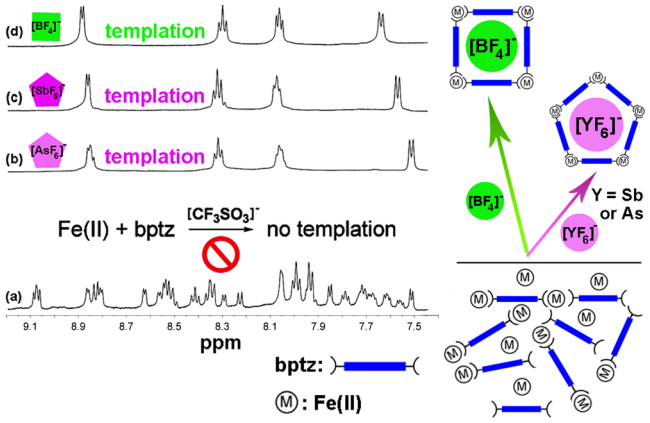

FIGURE 14. ^{1}H NMR spectra of $Fe(CF_3SO_3)_2$ with bptz in CD_3CN (a) upon addition of excess (b) $KAsF_6$ (c) $[n\text{-}Bu_4N][SbF_6]$ (d) $[n\text{-}Bu_4N][BF_4]$. Adapted with permission from ref 35. Copyright 2013 American Chemical Society.

TABLE 2. Average Distances (Å) in bptz Metallacycles

M(II)	cross-ligand (Å)	diagonal (Å)
	squares	
Fe(II)	6.5	9.1
Ni(II)	6.9	9.7
Co(II)	7.0	9.9
Zn(II)	7.2	10.1
	pentagons	
Fe(II)	6.4	10.4
Ni(II)	6.7	10.9

anions in the polygon formation and the close cavity contacts are also evident by considering the metallacycles with the octahedral pnictogen anions. As evidenced by ^{1}H NMR spectroscopy, MS, and CV studies, $[Fe_5(bptz)_5(CH_3CN)_{10}][PF_6]_{10}$ is templated by $[PF_6]^-$ in solution,[35] in contrast to Ni(II) ions which form neither pentagons nor squares supported by $[PF_6]^-$ anions.[33] The aforementioned difference may be explained by the fact that $[PF_6]^-$ ions establish closer anion–π interactions with the edges in the smaller Fe(II) cage as compared to the larger Ni(II) congener (Table 2). The Fe(II) pentagon with encapsulated $[PF_6]^-$ (54 Å^3), however, is relatively unstable, in contrast to that templated by $[AsF_6]^-$ (63 Å^3), which is even more stable than the Fe(II) pentagon templated by $[SbF_6]^-$ (71 Å^3) ions. As evidenced by ^{1}H NMR spectroscopic studies, conversion of $[Fe_4(bptz)_4(CH_3CN)_8][BF_4]_8$ to ~50:50 mixtures with $[Fe_5(bptz)_5(CH_3CN)_{10}][AsF_6]_{10}$ or $[Fe_5(bptz)_5(CH_3CN)_{10}][SbF_6]_{10}$ (Figure 13), by the addition of an excess of $[AsF_6]^-$ or $[SbF_6]^-$ ions, requires mere overnight stirring at 55 °C or refluxing for 2 days in CD_3CN, respectively (Scheme 2C).[35] Therefore, the order of stability for the Fe(II) pentagons is $[Fe_5(bptz)_5(CH_3CN)_{10}][PF_6]_{10} \ll [Fe_5(bptz)_5(CH_3CN)_{10}][SbF_6]_{10} < [Fe_5(bptz)_5(CH_3CN)_{10}][AsF_6]_{10}$, in accord with an enhanced synergistic effect arising from the anion–π contacts of the templating anion series with the cavity. Moreover, the fact that $[Fe_5(bptz)_5(CH_3CN)_{10}][SbF_6]_{10}$ is more stable than $[Ni_5(bptz)_5(CH_3CN)_{10}][SbF_6]_{10}$ and the lack of an observed Zn(II) congener templated by $[SbF_6]^-$ agrees well with the cavity size and metal bond lability, considering that the M-N distances contract in the order Zn(II) > Ni(II) ~ Co(II) ≫ Fe(II) (Table 2). These comparisons further corroborate the importance of optimal cavity/anion fit to enhance the short anion–π contacts that stabilize the metallacycles.[35] Remarkably, both $[Fe_4(bptz)_4(CH_3CN)_8][BF_4]_8$ and $[Fe_5(bptz)_5(CH_3CN)_{10}][SbF_6]_{10}$ exhibit higher than expected cavity occupancies by the guest anions,[35] which is achieved due to the enhanced stability provided by the short anion–π contacts (Table 1).

Of paramount importance to the preceding arguments are our recent ^{1}H NMR data, which provide strong evidence for templation of these polygons in solution. The bptz moieties form linear Fe(II) oligomeric mixtures with non-templating anions despite their appropriate size for templation, for example, $[CF_3SO_3]^-$;[35] self-assembly is activated and the building blocks are organized into an exclusive metallacycle, however, *only* upon addition of suitable templating anions, for example, $[BF_4]^-$, $[AsF_6]^-$ and $[SbF_6]^-$, which lead to $[Fe_4(bptz)_4(CH_3CN)_8][BF_4]_8$, $[Fe_5(bptz)_5(CH_3CN)_{10}][AsF_6]_{10}$, and $[Fe_5(bptz)_5(CH_3CN)_{10}][SbF_6]_{10}$, respectively (the onset of templation is evidenced by the characteristic symmetric ^{1}H NMR spectra for the corresponding closed polygons in CH_3CN; Figure 14).[35] The aforementioned results support our contention that the metallacycles do not form in the absence of templating anions and that the appropriate anionic templates are an essential part of the metallacycles.

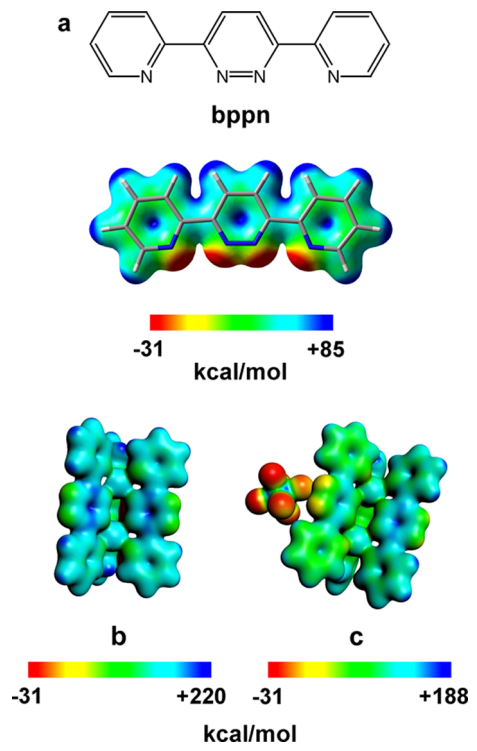

FIGURE 15. Schematic representation and ESP maps of (a) bppn calculated with B3LYP/6-31+G(d,p),[48] (b) $[Ag_2(bptz)_3]^{2+}$, and (c) $\{[Ag_2(bptz)_3][SbF_6]\}^+$ (from BP86/TZP SPE calculations). Parts (b) and (c) adapted with permission from ref 36. Copyright 2006 American Chemical Society.

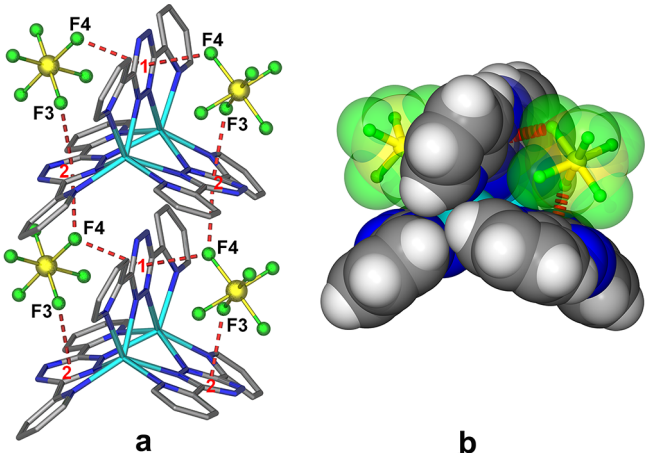

FIGURE 16. (a) Ball-and-stick and (b) space-filling representations for $[Ag_2(bptz)_3][SbF_6]_2$. Part (a) reprinted with permission from ref 36. Copyright 2006 American Chemical Society.

The ^{19}F NMR data also support the presence of anion-encapsulated metallacycles in solution. Broadening of the free anion ^{19}F NMR resonances between +20 and −40 °C for $[Zn_4(bptz)_4(CH_3CN)_8][BF_4]_8$, $[Fe_5(bptz)_5(CH_3CN)_{10}][PF_6]_{10}$, and $[Fe_4(bptz)_4(CH_3CN)_8][BF_4]_8$ indicates dynamic *endo/exo* exchange of the relevant anions in solution.[35] Furthermore,

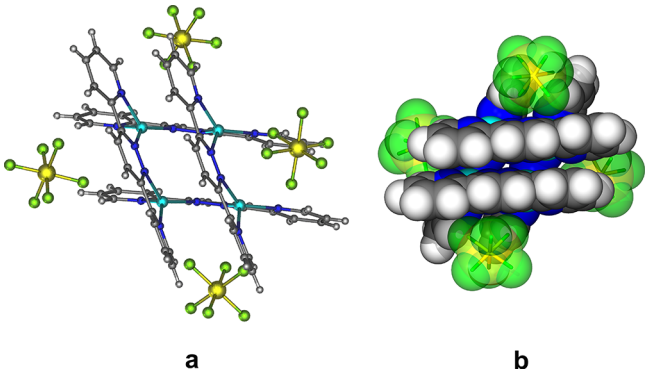

FIGURE 17. (a) Ball-and-stick and (b) space-filling representations for $[Ag_4(bppn)_4][SbF_6]_4$.[36]

TABLE 3. Anion−π Contacts in Ag(I)-bptz and Ag(I)-bppn Complexes[36]

compd	rings/anion with anion−π contacts	shortest F···centroid distance (Å)
$\{[Ag(bptz)][PF_6]\}_\infty$	2	2.840(5)
$[Ag_2(bptz)_2(CH_3CN)_2][PF_6]_2$	2	2.806(7)
$[Ag_2(bptz)_2(CH_3CN)_2][AsF_6]_2$	2	2.784(6)
$[Ag_2(bptz)_3][AsF_6]_2$	3	2.913(2)
$[Ag_2(bptz)_3][SbF_6]_2$[a]	3	2.913(6)
$[Ag_2(bptz)_3][SbF_6]_2$[a]	6	2.844[b]
$[Ag_4(bppn)_4][PF_6]_4$	1	3.095(6)
$[Ag_4(bppn)_4][AsF_6]_4$	1	3.096(3)
$[Ag_4(bppn)_4][SbF_6]_4$	1	3.260(5)
$[Ag_4(bppn)_4][BF_4]_4$	1	2.90(4)

[a]Two products from the same reaction. [b]F···tetrazine plane distance.

at low temperatures, the ^{19}F NMR spectra for $[Zn_4(bptz)_4(CH_3CN)_8][BF_4]_8$ or $[Fe_5(bptz)_5(CH_3CN)_{10}][PF_6]_{10}$ in CD_3CN, exhibit two resonances for each polygon ascribed to free and encapsulated $[BF_4]^-$ or $[PF_6]^-$ ions, respectively.[33,35] For $[Zn_4(bptz)_4(CH_3CN)_8][BF_4]_8$, the calculated anion exchange rate is $k_{exc(BF_4)} = \sim 140(14)\ s^{-1}$ (238 K) yielding an activation energy of encapsulation $\Delta G^{\ddagger}_{238K(BF_4)} = 48(4)$ kJ/mol and for $[Fe_5(bptz)_5(CH_3CN)_{10}][PF_6]_{10}$, $k_{exc(PF_6)} = 166(16)\ s^{-1}$ (233 K) and $\Delta G^{\ddagger}_{233K(PF_6)} = 46(4)$ kJ/mol.[35] The aforementioned low activation energy values (~50 kJ/mol) confirm that only diffusional exchange of the encapsulated anions occurs through the open faces of the intact metallacyclic cages, without M−N coordination bond cleavage, thereby reinforcing the contention that the encapsulated anions are embedded in the cavities by noncovalent anion−π interactions (~20−70 kJ/mol).[35]

5. Structural Motifs of Self-Assembled Ag(I) Complexes Dictated by Anion−π Interactions

Armed with the knowledge from the metallacycles, we undertook a comprehensive investigation of the reactions between the coordinatively flexible Ag(I) ion with X^- = $[PF_6]^-$, $[AsF_6]^-$, $[SbF_6]^-$, $[BF_4]^-$, and bptz or bppn, in order to assess the effect of varying the ligand π-acidity and

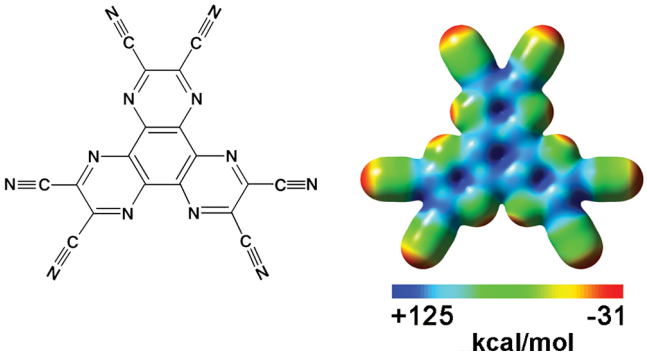

FIGURE 18. Schematic representation and ESP map of $HAT(CN)_6$. Adapted with permission from ref 23. Copyright 2010 John Wiley and Sons.

anion identity on the preferred resulting structural motifs.[36] As indicated by the ESP maps, the central rings of bptz and bppn exhibit different degrees of π-acidity with bptz displaying a significantly higher electropositive character of the tetrazine as compared to the more electron-rich pyridazine ring (Figures 6a, 15a). The higher π-acidity of tetrazine renders bptz amenable to anion–π rather than π–π interactions, which is reflected in the ensuing structural motifs of the Ag(I) complexes. The bptz reactions lead to polymeric, dinuclear, or propeller-type structures (Figure 16),[36,37] depending on the experimental conditions and anion present, whereas the bppn reactions give rise to grid-type structures $[Ag_4(bppn)_4]^{4+}$ regardless of the anion (Figure 17).[36]

In the case of the bppn grids, the π–π stacking is maximized at the expense of anion–π interactions, whereas in the bptz complexes multiple, shorter (by ~0.2 Å), and thus stronger anion–π interactions than those encountered in the bppn complexes are established (Table 3).[36] The most intriguing Ag(I)-bptz species are the propeller-type structures $[Ag_2(bptz)_3][SbF_6]_2$ (Figure 16) and $[Ag_2(bptz)_3][AsF_6]_2$ with three bptz rings spanning two metal centers and the anions embedded in the cation folds establishing short anion–π contacts with the tetrazine rings (three per anion).[36,37]

The evidence gleaned from the solid-state structures *vis-à-vis* the relative strength of anion–π interactions for the Ag(I)-bptz and Ag(I)-bppn complexes was corroborated by DFT single-point energy calculations, which revealed shifts in the ESP maps for the tetrazine rings in close contact with anions, for example, $\{[Ag_2(bptz)_3][SbF_6]\}^+$ versus $[Ag_2(bptz)_3]^{2+}$ (Figure 15b,c).[36]

6. Multisite Anion Interactions of the Extended π-Acidic Arene $HAT(CN)_6$

In highly π-acidic arenes, X-ray structural determinations and theoretical studies demonstrated that the anions are

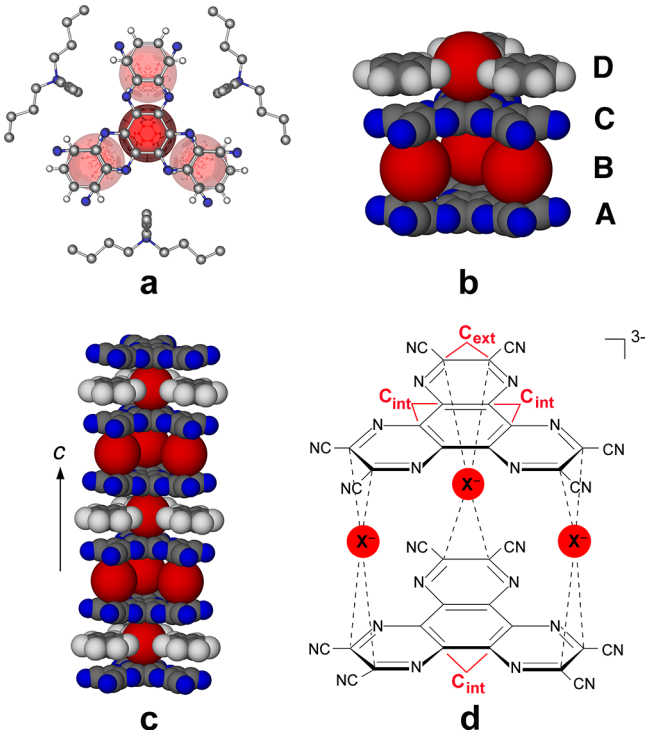

FIGURE 19. Repeat layers ABCD in $\{([n\text{-}Bu_4N][X])_3[HAT(CN)_6]_2\}\cdot 3C_6H_6$ ($X^- = Br^-, I^-$): (a) down, (b) along *c* axis, (c) vertical stacks, and (d) multisite anion contacts in $\{[HAT(CN)_6]_2[X]_3\}^{3-}$ in solution ($X^- = I^-, Br^-, Cl^-$). Adapted with permission from ref 23. Copyright 2010 John Wiley and Sons.

TABLE 4. Closest Contacts in $\{([n\text{-}Bu_4N][X])_3[HAT(CN)_6]_2\}\cdot 3C_6H_6$[23,49]

X^- [a]	$d_{X\text{-centroid}}$ (Å)	$X\cdots C_{ext}$ or R_{CT} (Å)
I^-	3.337[b,e]	3.334[b,e]
	3.419[c,e]	3.506[c,e]
	3.378[d]	3.420[d]
Br^-	3.245[b,e]	3.239[b,e]
	3.280[c,e]	3.354[c,e]
	3.262[d]	3.29[d]

[a]Each halide ion is in contact with two $HAT(CN)_6$ units. [b]Distance to layer A. [c]Distance to layer C. [d]Average value; ΣR_{vdW} C···Br 3.55 Å, ΣR_{vdW} C···I 3.68 Å. [e]η^2-contacts to C_{ext} (Figure 19).

preferentially located over the periphery of the rings (Figures 4b, 5) and that the interactions with the π-systems involve charge-transfer (CT), which in several cases is witnessed by the appearance of highly colored solutions or crystals.[23,41] Recently, a few cases involving chromogenic electron-transfer in the presence of strongly Lewis basic anions were reported.[24–26] We envisioned $HAT(CN)_6$ (Figure 18) to be a particularly attractive π-acidic heterocyclic system for establishing short contacts with anions,[23,49] due to the electron-withdrawing cyano groups, its high molecular polarizability, and positive quadrupole moment. Electronic, multinuclear NMR, and ESI-MS spectroscopies together with X-ray crystallography were applied to assess the strong

TABLE 5. Spectroscopic Features for $HAT(CN)_6$/Halide Associates[23]

	solvent	Cl^-	Br^-	I^-	solvent	Cl^-	Br^-	I^-
λ_{max} (nm)	THF	408	419	630	CH_3NO_2	390	406	557
K_{CT} $(M^{-1})^a$	THF	3780	2200	940	CH_3NO_2	71	48	20

[a] At 25 °C.

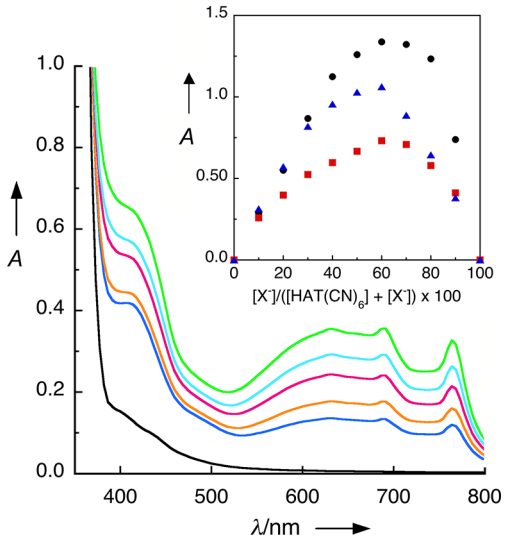

FIGURE 20. Spectral changes upon incremental additions of $[n\text{-}Bu_4N][I]$ (0−3.55 mM) to $HAT(CN)_6$ (0.130 mM) in THF. Inset: Job plots (black circles) chloride, (red squares) bromide, (blue triangles) iodide ions. Adapted with permission from ref 23. Copyright 2010 John Wiley and Sons.

association of the donor halide ions with the π-acceptor $HAT(CN)_6$.[23]

The cocrystallization of $HAT(CN)_6$ with $[n\text{-}Bu_4N][X]$ ($X^- = I^-$, Br^-) affords intensely colored crystals of the isostructural analogs $\{([n\text{-}Bu_4N][X])_3[HAT(CN)_6]_2\}\cdot 3C_6H_6$.[23,49] The stabilization and propagation of infinite chains $\{[HAT(CN)_6]_2[X]_3\}^{3-}\cdots[X^-]\cdots\{[HAT(CN)_6]_2[X]_3\}^{3-}\cdots[X^-]\cdots\{[HAT(CN)_6]_2[X]_3\}^{3-}$, consisting of layers ABCD, is governed by CT contacts between the halide donors to the peripheral C_{ext} atoms of the $HAT(CN)_6$ pyrazine rings as well as anion−π interactions at the core ring centroids (Figure 19). The CT interaction strength is indicated by the close peripheral halide η^2,η^2 contacts to C_{ext} at distances by up to 0.35 Å shorter than ΣR_{vdW} C···X (Table 4).[23] The shorter distances of the peripheral anions to C_{ext}, as compared to the central anions from C_{int} of the core rings, imply that the latter anion−π interactions are clearly weaker than the peripheral CT contacts in the complexes.[23]

In solution, the CT nature of the $HAT(CN)_6$/halide complexes ($X^- = Cl^-$, Br^-, I^-; THF or CH_3NO_2) was confirmed by the appearance of new prominent absorption bands in the visible region of the electronic spectra (Table 5; Figure 20),[50]

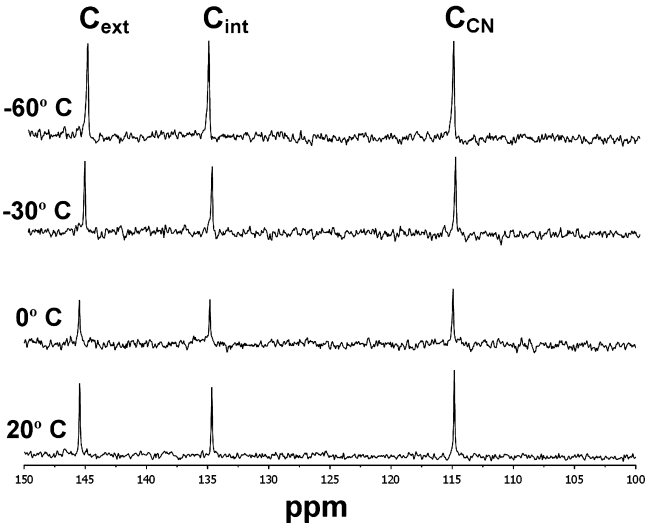

FIGURE 21. Variable Temperature ^{13}C NMR spectra for the $\{[HAT(CN)_6]_2[Br]_3\}^{3-}$ associates in THF-d_8.

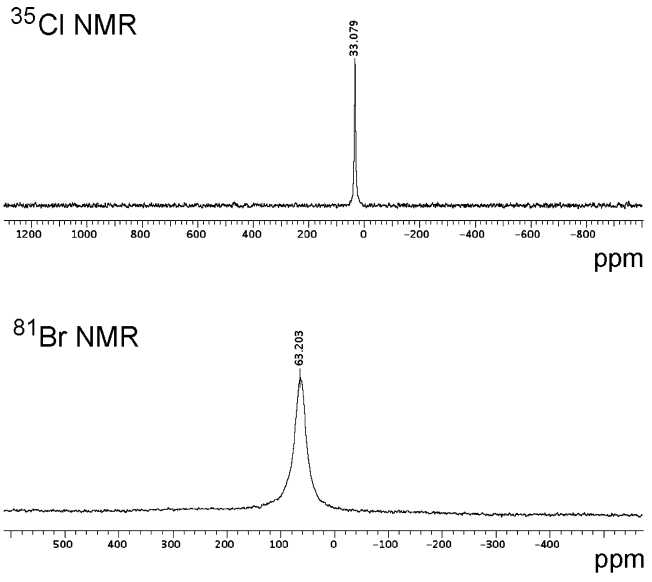

FIGURE 22. Halogen NMR spectra for the $\{[HAT(CN)_6]_2[X]_3\}^{3-}$ associates in CD_3NO_2-d_3 ($X^- = Cl^-$, Br^-).[23]

the dependence of the transition energies ($h\nu_{CT}$) on the solvent polarity and their linear correlation with the anodic potentials of the donors (Mulliken correlation).[23] The order of the complex association constants is $K_{CT,Cl} > K_{CT,Br} > K_{CT,I}$ and also $K_{CT,X}(CH_3NO_2) < K_{CT,X}(THF)$ (Table 5).[23] The unusually high $K_{CT,X}$(THF) values (2−5 times higher than typical CT complexes) speak to the high $HAT(CN)_6$/halide complex stability, which is attributed to the $HAT(CN)_6$ exceptional acceptor strength stemming from the electron-withdrawing cyano groups and the extensively delocalized π-aromatic system.

The spontaneous formation of $\{[HAT(CN)_6]_2[X]_3\}^{3-}$ CT assemblies in solution, with peripheral positioning of the

anions, is supported by Job plots (Figure 20, inset), which support a 2:3 stoichiometric ratio for $[HAT(CN)_6]$:[X] ($X^- = Cl^-$, Br^-, I^-; Figure 19d).[23] Furthermore, the aromatic region for each complex in THF-d_8 or CD_3NO_2-d_3 exhibits three ^{13}C NMR resonances corresponding to the peripheral C_{ext}, central C_{int}, and −CN carbon atoms (Figure 21), which indicate that the positions of the halide ions are related by a C_3 rotation axis. These findings are in accord with three anions being positioned over the $C_{ext}-C_{ext}$ bonds in a η^2-fashion, in agreement with the findings from the solid-state data (Figure 19d).[23] Additionally, the retention of three resonances in the ^{13}C NMR spectra of each complex at low temperatures (Figure 21) indicates that one anion is not shared among the three $C_{ext}-C_{ext}$ positions. The C_{ext} resonances exhibit downfield shifts $\Delta\delta_{ext} \sim 1-3$ ppm, as compared to $HAT(CN)_6$, which support the presence of CT contacts with the halide ions.[23]

Despite the challenge of appreciable nuclear quadrupole moments for halogen nuclei ($I > 1/2$), we succeeded in also corroborating the aforementioned contacts by recording halogen NMR spectra (Figure 22), which revealed substantial downfield-shifted ^{35}Cl, ^{81}Br, and ^{127}I resonances for the complexes $\{[HAT(CN)_6]_2[X]_3\}^{3-}$ $\{\Delta\delta\ (^{35}Cl) > \Delta\delta\ (^{81}Br) > \Delta\delta\ (^{127}I)\}$ as compared to the corresponding free halide salts;[23] these shifts are indicative of one type of halide interaction in each complex and deshielding of the donor nuclei due to CT, thus confirming the structure depicted in Figure 19d in solution.

Other relevant notable systems that hold great promise in many applications, are the template directed mechanically interlocked molecules reported by Stoddart and Griffiths, exhibiting noncovalent donor−acceptor interactions between π-electron-rich and π-electron-deficient macrocycles.[51]

7. Concluding Remarks

The findings highlighted herein attest to the fact that anions in close contact with π-acidic aromatic ligands trigger the assembly and play a salient role in stabilizing cationic metallasupramolecular architectures. The subtle interplay between anions, ring π-acidity, and metal ions, in synergy with prominent anion−π contacts, dictates the outcome of the anion-templated processes in the solid state and in solution. Our studies unequivocally demonstrate that additive anion−π interactions are responsible for the template effect in rare metallacycles despite counterintuitive nuclearities (pentagons); the stability of the ensuing architectures was correlated with the encapsulated anion−π contact strength. In a relevant assessment of ligand π-acidity and the self-assembly outcome, the influence of enhanced short anion−π contacts is reflected in the formation of propeller versus grid-type entities.

Unprecedented multisite CT interactions observed for the distinctly colored $HAT(CN)_6$/halide 1D complexes in the solid state and in solution also lend credence to the importance of short anion contacts in dictating supramolecular architectures and bode well for their use as anion-sensing receptors. The aforementioned self-assembled systems showcase anion−π contacts at the forefront of novel supramolecular interactions and pave the way to an understanding of their fundamental nature in solution and the solid state as well as for unearthing other intriguing synthetic or natural frameworks directed by them.

K.R.D. gratefully acknowledges the Robert A. Welch Foundation (A-1449). We thank the former graduate students Drs. Ian D. Giles, Brandi L. Schottel, and Christian Saul Campos-Fernández for their contributions to the research described herein.

BIOGRAPHICAL INFORMATION

Kim R. Dunbar was born in Mount Pleasant, PA, and received a B.S. from Westminster College (1980) and a Ph.D. from Purdue University (1984). She is a former faculty member of MSU (1987), is currently a Distinguished Professor at Texas A&M University, and holds the Davidson Chair of Science. Her research spans topics in synthetic and structural inorganic chemistry with a focus on the design of conducting and magnetic molecular materials, and antitumor properties of metal complexes. She is a past Alfred Sloan Foundation Fellow, a Camille Henry Dreyfus Teacher-Scholar, and an AAAS and ACS Fellow. Her honors include Distinguished Alumna Awards and an honorary degree (Westminster College; Purdue University), a Distinguished Faculty Award (MSU), and Graduate Mentoring and Research Awards (TAMU). She is an Associate Editor for *Inorganic Chemistry*.

Helen T. Chifotides was born in Providence, RI, and received her B.S. and Ph.D. in Chemistry from the University of Athens, Greece. After a NATO Postdoctoral Fellowship at Michigan State University (1995), she was appointed as Chemistry Lecturer at Oregon State University (1996). She held a senior staff scientist position in the Biochemistry Laboratory of the Pulmonary Hospital (Greece) until 2001. Currently, she is a Research Scientist at Texas A&M University. Her research interests span anticancer metal complexes with DNA and other biologically active molecules as well as noncovalent interactions in supramolecular chemistry.

FOOTNOTES

*To whom correspondence should be addressed.E-mail: chifotides@mail.chem.tamu.edu; dunbar@mail.chem.tamu.edu.

The authors declare no competing financial interest.

REFERENCES

1 Salonen, L. M.; Ellermann, M.; Diederich, F. Aromatic Rings in Chemical and Biological Recognition: Energetics and Structures. *Angew. Chem., Int. Ed.* **2011**, *50*, 4808–4842.

2 Zacharias, N.; Dougherty, D. A. Cation-π Interactions in Ligand Recognition and Catalysis. *Trends Pharmacol. Sci.* **2002**, *23*, 281–287.

3 Quiñonero, D.; Garau, C.; Rotger, C.; Frontera, A.; Ballester, P.; Costa, A.; Deyà, P. M. Anion-π Interactions: Do They Exist? *Angew. Chem., Int. Ed.* **2002**, *41*, 3389–3392.

4 Hiraoka, K.; Mizuse, S.; Yamabe, S. High-Symmetric Structure of the Gas-Phase Cluster Ions $X^- \cdots C_6F_6$ (X = Cl, Br, I). *J. Phys. Chem.* **1987**, *91*, 5294–5297.

5 Schneider, H.-J. Binding Mechanisms in Supramolecular Complexes. *Angew. Chem., Int. Ed.* **2009**, *48*, 3924–3977.

6 Mascal, M.; Armstrong, A.; Bartberger, M. D. Anion-Aromatic Bonding: A Case for Anion Recognition by π-Acidic Rings. *J. Am. Chem. Soc.* **2002**, *124*, 6274–6276.

7 Alkorta, I.; Rozas, I.; Elguero, J. Interactions of Anions with Perfluoro Aromatic Compounds. *J. Am. Chem. Soc.* **2002**, *124*, 8593–8598.

8 Schottel, B. L.; Chifotides, H. T.; Dunbar, K. R. Anion-π Interactions. *Chem. Soc. Rev.* **2008**, *37*, 68–83.

9 Frontera, A.; Gamez, P.; Mascal, M.; Mooibroek, T. J.; Reedijk, J. Putting Anion-π Interactions in Perspective. *Angew. Chem., Int. Ed.* **2011**, *50*, 9564–9583.

10 Gamez, P.; Mooibroek, T. J.; Teat, S. J.; Reedijk, J. Anion Binding Involving π-Acidic Heteroaromatic Rings. *Acc. Chem. Res.* **2007**, *40*, 435–444.

11 Mooibroek, T. J.; Black, C. A.; Gamez, P.; Reedijk, J. What's New in the Realm of Anion-π Binding Interactions? Putting Anion-π Interactions in Perspective. *Cryst. Growth Des.* **2008**, *8*, 1082–1093.

12 Berryman, O. B.; Johnson, D. W. Experimental Evidence for Interactions Between Anions and Electron-Deficient Aromatic Rings. *Chem. Commun.* **2009**, 3143–3153.

13 Wenzel, M.; Hiscock, J. R.; Gale, P. A. Anion Receptor Chemistry: Highlights from 2010. *Chem. Soc. Rev.* **2012**, *41*, 480–520.

14 (a) Estarellas, C.; Frontera, A.; Quiñonero, D.; Deyà, P. M. Anion-π Interactions in Flavoproteins. *Chem.—Asian J.* **2011**, *6*, 2316–2318. (b) Estarellas, C.; Frontera, A.; Quiñonero, D.; Deyà, P. M. Relevant Anion-π Interactions in Biological Systems: The Case of Urate Oxidase. *Angew. Chem., Int. Ed.* **2011**, *50*, 415–418.

15 (a) Philip, V.; Harris, J.; Adams, R.; Nguyen, D.; Spiers, J.; Baudry, J.; Howell, E. E.; Hinde, R. J. A Survey of Aspartate-Phenylalanine and Glutamate-Phenylalanine Interactions in the Protein Data Bank: Searching for Anion-π Pairs. *Biochemistry* **2011**, *50*, 2939–2950. (b) Jenkins, D. D.; Harris, J.; Howell, E. E.; Hinde, R. J.; Baudry, J. STAAR: Statistical Analysis of Aromatic Rings. *J. Comp. Chem.* **2013**, *34*, 518−522.

16 Robertazzi, A.; Krull, F.; Knapp, E.-W.; Gamez, P. Recent Advances in Anion-π Interactions. *CrystEngComm* **2011**, *13*, 3293–3300.

17 Krieger, I. V.; Freundlich, Joel S.; Gawandi, V. B.; Roberts, J. B.; Gawandi, V. B.; Sun, Q.; Owen, J. L.; Fraile, M. T.; Huss, S. I.; Lavandera, J.-L.; Ioerger, T. R.; Sacchettini, J. C. Structure-Guided Discovery of Phenyl-diketo Acids as Potent Inhibitors of *M. tuberculosis* Malate Synthase. *Chem. Biol.* **2012**, *19*, 1556–1567.

18 Matter, H.; Nazaré, M.; Güssregen, S.; Will, D. W.; Schreuder, H.; Bauer, A.; Urmann, M.; Ritter, K.; Wagner, M.; Wehner, V. Evidence of C-Cl/C-Br$\cdots\pi$ Interactions as an Important Contribution to Protein-Ligand Binding Affinity. *Angew. Chem., Int. Ed.* **2009**, *48*, 2911–2916.

19 Egli, M.; Sarkhel, S. Lone Pair Aromatic Interactions: To Stabilize or Not to Stabilize? *Angew. Chem., Int. Ed.* **2007**, *40*, 197–205.

20 Jentzsch, A. V.; Emery, D.; Mareda, J.; Metrangolo, P.; Resnati, G.; Matile, S. Ditopic Ion Transport Systems: Anion-π Interactions and Halogen Bonds at Work. *Angew. Chem., Int. Ed.* **2011**, *50*, 11675–11678.

21 Chudzinski, M. G.; McClary, C. A.; Taylor, M. S. Anion Receptors Composed of Hydrogen- and Halogen-Bond Donor Groups: Modulating Selectivity with Distinct Noncovalent Interactions. *J. Am. Chem. Soc.* **2011**, *133*, 10559–10567.

22 Ballester, P. Experimental Quantification of Anion-π Interactions in Solution Using Neutral Host-Guest Model Systems. *Acc. Chem. Res.* **2012**, DOI: 10.1021/ar300080f.

23 Chifotides, H. T.; Schottel, B. L.; Dunbar, K. R. The π-Accepting Arene $HAT(CN)_6$ as a Halide Receptor through Charge Transfer: Multisite Anion Interactions and Self-Assembly in Solution and the Solid State. *Angew. Chem., Int. Ed.* **2010**, *49*, 7202–7207.

24 (a) Guha, S.; Saha, S. Fluoride Ion Sensing by an Anion−π Interaction. *J. Am. Chem. Soc.* **2010**, *132*, 17674–17677. (b) Guha, S.; Goodson, F. S.; Corson, L. J.; Saha, S. Boundaries of Anion/Naphthalenediimide Interactions: From Anion−π Interactions to Anion-Induced Charge-Transfer and Electron-Transfer Phenomena. *J. Am. Chem. Soc.* **2012**, *134*, 13679–13691.

25 Aragay, G.; Frontera, A.; Lloveras, G.; Vidal-Gancedo, J; Ballester, P. Different Nature of the Interactions Between Anions and $HAT(CN)_6$: From Reversible Anion-π Complexes to Irreversible Electron-Transfer Processes. *J. Am. Chem. Soc.* **2013**, *135*, 2620−2627.

26 Zhao, Y.; Li, Y.; Qin, Z.; Jiang, R.; Liu, H.; Li, Y. Selective and Colorimetric Anion Chemosensor Based on *s*-Tetrazines. *Dalton Trans.* **2012**, *41*, 13338–13342.

27 Mascal, M.; Yakovlev, I.; Nikitin, E. B.; Fettinger, J. C. Fluoride-Selective Host Based on Anion−π Interactions, Ion Pairing and Hydrogen Bonding: Synthesis and Fluoride-Ion Sandwich Complex. *Angew. Chem., Int. Ed.* **2007**, *46*, 8782–8784.

28 Perraud, O.; Robert, V.; Gornitzka, H.; Martinez, A.; Dutasta, J.-P. Combined Cation-π and Anion-π Interactions for Zwitterion Recognition. *Angew. Chem., Int. Ed.* **2012**, *51*, 504–508.

29 (a) Wang, D.-X.; Wang, M.-X. Anion Recognition by Charge Neutral Electron-Deficient Arene Receptors. *Chimia* **2011**, *65*, 939–943. (b) Wang, D.-X.; Wang, M. X. Anion-π Interactions: Generality, Binding Strength and Structure. *J. Am. Chem. Soc.* **2013**, *135*, 892−897.

30 Chakravarty, S.; Sheng, Z.-Z.; Iverson, B.; Moore, B. η^6-Type Anion-π in Biomolecular Recognition. *FEBS Letters,* **2012**, *586*, 4180–4185.

31 Misek, J.; Jentzsch, A. V.; Sakurai, S.; Emery, D.; Mareda, J.; Matile, S. A. Chiral and Colorful Redox Switch: Enhanced π-Acidity in Action. *Angew. Chem., Int. Ed.* **2010**, *49*, 7680–7683.

32 (a) Dawson, R. E.; Hennig, A.; Weimann, D. P.; Emery, D.; Ravikumar, V.; Montenegro, J.; Takeuchi, T.; Gabutti, S.; Mayor, M.; Mareda, J.; Schalley, C. A.; Matile, S. Experimental Evidence for the Functional Relevance of Anion-π Interactions. *Nat. Chem.* **2010**, *2*, 533–538. (b) Mareda, J.; Matile, S. Anion-π Slides for Transmembrane Transport. *Chem. Eur. J.* **2009**, *15*, 28–37. (c) Gorteau, V.; Bollot, G.; Mareda, J.; Perez-Velasco, A.; Matile, S. *J. Am. Chem. Soc.* **2006**, *128*, 14788–14789.

33 Campos-Fernández, C. S.; Schottel, B. L.; Chifotides, H. T.; Bera, J. K.; Bacsa, J.; Koomen, J. M.; Russell, D. H.; Dunbar, K. R. Anion Template Effect on the Self-Assembly and Interconversion of Metallacyclophanes. *J. Am. Chem. Soc.* **2005**, *127*, 12909–12923.

34 Giles, I. D.; Chifotides, H. T.; Shatruk, M.; Dunbar, K. R. Anion-Templated Self-Assembly of Highly Stable Fe(II) Pentagonal Metallacycles with Short Anion-π Contacts. *Chem. Commun.* **2011**, *47*, 12604–12606.

35 Chifotides, H. T.; Giles, I. D.; Dunbar, K. R. Supramolecular Architectures with π-Acidic 3,6-Bis(2-pyridyl)-1,2,4,5-tetrazine Cavities: Role of Anion−π Interactions in the Remarkable Stability of Fe(II) Metallacycles in Solution. *J. Am. Chem. Soc.* **2013**, *135*, 3039−3055.

36 Schottel, B. L.; Chifotides, H. T.; Shatruk, M.; Chouai, A.; Bacsa, J.; Pérez, L. M.; Dunbar, K. R. Anion−π Interactions as a Controlling Element in Self-Assembly Reactions of Ag(I) Complexes with π-Acidic Aromatic Rings. *J. Am. Chem. Soc.* **2006**, *128*, 5895–5912.

37 Schottel, B. L.; Bacsa, J.; Dunbar, K. R. Anion Dependence of Ag(I) Reactions with 3,6-Bis(2-pyridyl)-1,2,4,5-tetrazine: Isolation of the Molecular Propeller $[Ag_2(bptz)_3][AsF_6]_2$. *Chem. Commun.* **2005**, 46–47.

38 Wheeler, S. E. Understanding Substituent Effects in Noncovalent Interactions Involving Aromatic Rings. *Acc. Chem. Res.*, **2012**, DOI: 10.1021/ar300109n.

39 Berryman, O. B.; Bryantsev, V. S.; Stay, D. P.; Johnson, D. W.; Hay, B. P. Structural Criteria for the Design of Anion Receptors: The Interaction of Halides with Electron-Deficient Arenes. *J. Am. Chem. Soc.* **2007**, *129*, 48–58.

40 Hay, B. P.; Bryantsev, V. S. Anion-Arene Adducts: C-H Hydrogen Bonding, Anion-π Interaction, and Carbon Bonding Motifs. *Chem. Commun.* **2008**, 2417–2428.

41 Rosokha, S. V.; Kochi, J. K. X-Ray Structures and Electronic Spectra of π-Halogen Complexes between Halogen Donors and Acceptors with π-Receptors. *Struct. Bonding (Berlin, Ger.)* **2008**, *126*, 137–160.

42 Smulders, M. M. J.; Riddell, I. A.; Browne, C.; Nitschke, J. R. Building on Architectural Principles for Three-dimensional Metallosupramolecular Construction. *Chem. Soc. Rev.* **2013**, *42*, 1728–1754.

43 Chakrabarty, R.; Mukherjee, P. S.; Stang, P. J. Supramolecular Coordination: Self-Assembly of Finite Two- and Three-Dimensional Ensembles. *Chem. Rev.* **2011**, *111*, 6810–6918.

44 Vilar, R. Anion-Templated Synthesis. *Angew. Chem., Int. Ed.* **2003**, *42*, 1460–1477.

45 Campos-Fernández, C. S.; Clérac, R.; Koomen, J. M.; Russell, D. H.; Dunbar, K. R. Fine-Tunning the Ring-Size of Metallacyclophanes: A Rational Approach to Molecular Pentagons. *J. Am. Chem. Soc.* **2001**, *123*, 773–774.

46 Campos-Fernández, C. S.; Clérac, R.; Dunbar, K. R. A One Pot High Yield Synthesis of a Paramagnetic Nickel Square from Divergent Precursors by Anion Template Assembly. *Angew. Chem., Int. Ed.* **1999**, *38*, 3477–3479.

47 Bu, X.-H.; Morishita, H.; Tanaka, K.; Biradha, K.; Furusho, S.; Shionoya, M. A Spontaneously Resolved Chiral Molecular Box: A Cyclic Tetranuclear Zn^{II} Complex with DPTZ. *Chem. Commun.* **2000**, 971–972.

48 Giles, I. D. Experimental and Theoretical Investigations of Anion-π Interactions in Metallacyclic Architectures of First-Row Transition Metals with N-Heteroaromatic Ligands. Ph.D. Dissertation, Texas A&M University, College Station, TX, 2012.

49 Szalay, P. S.; Galán-Mascarós, J. R.; Schottel, B. L.; Bacsa, J.; Pérez, L. M.; Ichimura, A. S.; Chouai, A.; Dunbar, K. R. Experimental and Computational Studies of Charge-Transfer and Reduction Products of 1,4,5,8,9,12-Hexaazatriphenylene-Hexacarbonitrile: $HAT(CN)_6$. *J. Cluster Sci.* **2004**, *15*, 503–530.

50 The additional low-intensity absorption bands that appear in the electronic spectra of the halide complexes at $\sim$ 762 and 685 nm (Figure 20, ref. 23) are attributed to small amounts of the radical anion $[HAT(CN)_6]^-$.

51 Griffiths, K. E.; Stoddart, J. F. Template-directed Synthesis of Donor/acceptor [2]Catenanes and [2]Rotaxanes. *Pure Appl. Chem.* **2008**, *80*, 485–506.